Chymase uptake by cardiomyocytes results in myosin degradation in cardiac volume overload

Pamela C. Powell [a], **Chih-Chang Wei** [a,b], **Lianwu Fu** [a,c], **Betty Pat** [a,b],
Wayne E. Bradley [a,b], **James F. Collawn** [c], **Louis J. Dell'Italia** [a,b,c,*]

[a] *Birmingham Veteran Affairs Medical Center, USA*

[b] *Division of Cardiovascular Disease, Department of Medicine, USA*

[c] *Department of Cell, Developmental and Integrative Biology, University of Alabama at Birmingham, Birmingham, AL, USA*

[*] Corresponding author.
E-mail address: louis.dellitalia@va.gov (L.J. Dell'Italia).

Abstract

Background: Volume overload (VO) of isolated mitral regurgitation (MR) or aortocaval fistula (ACF) is associated with extracellular matrix degradation and cardiomyocyte myofibrillar and desmin breakdown. Left ventricular (LV) chymase activity is increased in VO and recent studies demonstrate chymase presence within cardiomyocytes. Here we test the hypothesis that chymase within the cardiomyocyte coincides with myosin and desmin breakdown in VO.

Methods and results: Aortocaval fistula (ACF) was induced in Sprague Dawley (SD) rats and was compared to age-matched sham-operated rats at 24 hours, 4 and 12 weeks. Immunohistochemistry (IHC) and transmission electron microscopy (TEM) immunogold of LV tissue demonstrate chymase within cardiomyocytes at all ACF time points. IHC for myosin demonstrates myofibrillar disorganization starting at 24 hours. Proteolytic presence of chymase in cardiomyocytes is verified by *in situ* chymotryptic tissue activity that is inhibited by pretreatment with a chymase inhibitor. Real-time PCR of isolated cardiomyocytes at all ACF time points and *in situ* hybridization demonstrate

endothelial cells and fibroblasts as a major source of chymase mRNA in addition to mast cells. Chymase added to adult rat cardiomyocytes *in vitro* is taken up by a dynamin-mediated process and myosin breakdown is attenuated by dynamin inhibitor, suggesting that chymase uptake is essential for myosin breakdown. In a previous study in the dog model of chronic MR, the intracellular changes were attributed to extracellular effects. However, we now demonstrate intracellular effects of chymase in both species.

Conclusion: In response to VO, fibroblast and endothelial cells produce chymase and subsequent cardiomyocyte chymase uptake is followed by myosin degradation. The results demonstrate a novel intracellular chymase-mediated mechanism of cardiomyocyte dysfunction and adverse remodeling in a pure VO.

Keywords: Cardiology, Cell biology, Molecular biology

1. Introduction

The volume overload (VO) of isolated mitral regurgitation (MR) or aortocaval fistula (ACF) is a pure stretch on the myocardium coupled with a facilitated LV ejection into the left atrium or ACF. Chronic pure VO results in LV dilatation that is associated with a loss/breakdown of extracellular matrix (ECM) and is exacerbated by the antifibrotic effects of renin-angiotensin system blockers [1, 2, 3, 4, 5]. In addition to an increase in mast cells in VO, we have demonstrated fibroblast production of chymase that results in intracellular autophagic breakdown of procollagen and fibronectin in the rat [6]. There is also a concomitant breakdown of cardiomyocyte myofibrils and the major intermediate filament desmin [7, 8, 9]. Thus, extracellular and intracellular structural protein breakdown is the underpinning of cardiomyocyte elongation and thinning that translates to LV spherical dilatation and wall thinning.

The serine protease chymase is upregulated in the pure VO of MR in the dog [1, 10, 11], ACF in the rat [4, 5, 6] and mouse [12], and in the human MR left atrium with left-sided heart disease and MR [13]. Chymase is a highly efficient Angiotensin II (Ang II)-forming enzyme, but its multifunctional protease actions lead to activation of MMPs, IL-6, IL-1β and kallikrein, in addition to digestion of fibronectin and laminin [14]. All of these effects in VO have been attributed to chymase's extracellular actions. However, identification of chymase within human left atrial myocytes in left-sided heart disease [13] and in the dog with ischemia reperfusion injury [15] has opened up an entirely new possibility for chymase's destructive protease actions within the cardiomyocyte.

Largely thought to be the product of mast cells, the identification of other cellular sources including cardiac fibroblasts and vascular endothelial cells demonstrate the potential for a more widely dispersed chymase production and distribution in

various tissues. However, intracellular cardiomyocyte targets and activity are unknown and whether the cardiomyocyte produces chymase remains an open question. Further, the multiple rodent β-isoforms of rat mast cell proteases (rMCP) that degrade Ang II, in addition to the Ang II-forming α isoform, confound the direct clinical application to the human in which there is only the α-isoform [16]. We chose to focus on rMCP-2 due to its sequence homology to rat smooth muscle chymase which is largely Ang II generating [17]. Thus, in the current investigation, we address these questions using *in vivo* and *in vitro* approaches to demonstrate that during VO, multiple cellular sources of rMCP-2 in addition to mast cells result in an increase in intracellular cardiomyocyte rMCP-2 and myosin breakdown.

2. Methods

2.1. Animal preparation

Adult male Sprague-Dawley rats (200−250 g) at 12 weeks of age were subjected to either sham or ACF surgery as described previously in our laboratory [3, 4, 5, 6, 7, 8]. The animal use in these studies was approved by the University of Alabama at Birmingham Animal Resource Program (Protocol 130409070). The dog LV tissue utilized in this study was obtained from mongrel dogs (19−26 kg) who underwent induction of mitral regurgitation (MR) by closed chest mitral valvular chordal rupture as previously described in our laboratory [18]. Dogs had 4 months of untreated MR or 4 months of MR treated with chymase inhibitor (CI) (4-{1-[(4-methylbenzo[6] thiophen-3-yl)methyl]benzimidazole-2-ylthio}butanoic acid, TEI-F00806; Teijin Pharma Ltd, Tokyo, Japan, at a dose of 100 mg/kg PO twice daily) [18] that was started 24 hours after MR induction.

2.2. Isolation of rat LV cardiomyocytes

Cardiomyocytes were isolated from sham and ACF rats as described previously in our laboratory [6, 7]. Briefly, hearts were perfused with perfusion buffer (120 mM NaCl, 15 mM KCl, 0.5 mM KH_2PO_4, 5 mM $NaHCO_3$, 10 mM HEPES, and 5 mM glucose, pH 7.0) for 5 minutes and digested with perfusion buffer containing 1 mg/mL collagenase II (Invitrogen, Carlsbad, CA) for 30 minutes at 37 °C. The right ventricle, atria and apex were removed before the perfused-heart was minced. The digestion was filtered, washed, and cells were pelleted. Only samples with >80% viability (indicated by healthy rod-shaped cells) were used.

2.3. Immunohistochemistry

Rat hearts were immersion-fixed in 10% neutral-buffered formalin and paraffin embedded. Sections (5 μm) were mounted on + slides, deparaffinized in xylene,

and rehydrated in a gradient series of ethanol. Sections used for fluorescent imaging were blocked with 5% goat serum and 1% bovine serum in phosphate buffered saline, and incubated overnight at 4 °C with the following primary antibodies: rMCP-2 mouse monoclonal line 3F4.5 (1:500, custom) and the corresponding rabbit polyclonal (1:250, custom); mouse anti-human chymase (1:50, Abcam ab2377); rabbit polyclonal desmin (1:200, Abcam ab15200); mouse myosin (1:10, Developmental Studies Hybridoma Bank (DSHB, University of Iowa) MF-20); Von Willebrand Factor (1:150, Chemicon 7356).

Dog hearts were prepared as described above. The following primary antibodies included rabbit polyclonal anti-human chymase (1:300, Bioss bs-2353R); mouse myosin (1:10, DSHB; MF-20), rabbit polyclonal desmin (1:200, Abcam ab15200) and the mouse monoclonal desmin (1:100, Abcam ab6322).

Alexa Fluor 488- and 594-conjugated secondary antibodies (1:700; Life Technologies/Invitrogen (Eugene, OR) with the appropriate host combinations were used. Nuclei (blue) were stained with DAPI (1.5 µg/mL; Vector Laboratories, Burlingame, CA, USA). Image acquisition was performed on a Leica DM6000 epifluorescence microscope with Simple-PCI software (Compix, Cranberry Township, PA, USA). Images were adjusted appropriately to remove background fluorescence.

2.4. Immunogold transmission electron microscopy

Immunogold electron microscopy was used to detect the localization of chymase at the ultrastructural level. The LV tissue pieces were submerged in 0.5% glutaraldehyde/3% paraformaldehyde in cardioplegic buffer (5% dextrose, 30 mM potassium chloride in phosphate buffered saline (PBS)), further fixed in the same fixative in cacodylate buffer, incubated in 0.1M glycine/PBS, dehydrated in series of N,N-dimethyl formamide, and embedded in LR White resin. Ultrathin (90 nm) sections [8] were picked up on nickel grids (3 mm), dried, and etched in a 3% solution of sodium m-periodate in 0.1N HCl 2 times for 30 minutes. Before immunolabeling, grids were rinsed 3 times in PBS and blocked for 1.5 hours with 1% BSA/1% goat serum/0.1% cold water fish skin gelatin/0.1% tween-20 in PBS. Grids were incubated with the rMCP-2 rabbit polyclonal antibody, diluted 1:25 with 1% BSA/PBS for 2 hours at room temperature and then overnight at 4 °C. The grids were rinsed with PBS 4 times, blocked in 1% BSA/1% goat serum in PBS 1.5 hours, and incubated (at room temperature for 2 hours) with goat anti-rabbit immunoglobulin G tagged with colloidal gold (10-nm particle size, diluted 1:50 with 1% BSA/PBS) (Aurion/Electron Microscopy Sciences). Sections were post fixed, counterstained with uranyl acetate and viewed on a FEI-Tecnai T12 Spirit 20 electron microscope at 120 kv.

2.5. Enzyme histochemistry

In situ chymotryptic-like activity staining was performed on rat LV tissue as previously described with the following modifications [19, 20]. Fresh tissue was immersion fixed in 4% paraformaldehyde 6 hours at room temperature, transferred to 25% sucrose overnight at 4 °C, then embedded in OCT compound (Tissue-Tek). Fixed-frozen 5 μm sections (cut within a week prior to tissue staining and kept stored at -80 °C) were thawed at room temperature, washed 3 times in PBS for 5 minutes each, and incubated in Reaction mixture (see below) at 37 °C for 3 hours. Sections were individually rinsed under running tap water for several minutes then counter-stained with Basic Fuchsin (0.05%) for 1−2 seconds to achieve a pale pink background, and immediately viewed under bright field microscopy. Mast cells stained intensely blue with chymase/esterase-positive granules and served as a positive control. Chymotryptic activity staining in the tissue/myocytes appeared as punctate blue dots on a pale pink background. Staining was inhibited with the chymase inhibitor TEI-F00806 at 50 μM.

Reaction mixture (100 ml) consisted of 0.53 mM Napthol AS-D chloroacetate (MP Biomedical), 0.3 mM Fast Blue BB Salt (Sigma) dissolved in N,N-Dimethylformamide (Sigma, final 3.8% in 100 ml) vortexed then immediately added to 50 mM Tris-Cl pH 7.5 (Fisher), 40 mM NaF (Acros Organics), and 1% Triton X-100 (Fisher) and allowed to stir for 2−3 minutes until a dark blue color appeared. The solution was filtered and used immediately.

2.6. In situ hybridization

The expression of rMCP-2 mRNA (rMcpt2) in the left ventricles of ACF rats was detected by *in situ* hybridization. The rMcpt2 cDNA flanked by the BamHI and NotI restriction sites (sequence was shown below) were synthesized and cloned to the pBluescript II KS(+) vector through the service provided by GenScript (Piscataway, NJ, USA). The resulting construct was confirmed by sequencing. The anti-sense and sense probes were synthesized with a digoxigenin (DIG) RNA labeling kit (Roche, 11175025910) utilizing the T7 and T3 RNA polymerase promoter in the pBluescript II KS(+) vector, respectively.

GGATCCGCCACCATGCAGGCCCTACTATTCCTGATGGCTCTTCTCTTGC
CTTCTGGAGCTGGAGCTGAGGAAATTATCGGTGGTGTGGAGTCTATTCC
TCACTCCCGCCCTTACATGGCCCATCTGGACATCGTCACTGAGAAAGGT
TTAAGGGTCATCTGTGGTGGGTTTCTCATAAGCCGTCAATTTGTGCTGA
CTGCTGCACATTGTAAAGGAAGAGAAATCACAGTCATCCTTGGAGCCC
ATGATGTGAGAAAGCGAGAATCCACACAGCAGAAGATAAAAGTC-

GAAAAACAAATCATTCACGAAAGTTACAACTCCGTTCCCAATCTTCAT-
GACATCATGTTACTGAAGCTTGAAAAAAAGTTGAGTTGACTCCTGCT
GTGAATGTAGTTCCTCTGCCCAGTCCCTCTGACTTTATCCACCCTGGGG-
CAATGTGTTGGGCAGCTGGATGGGGGAAAACTGGAGTTAGAGATCC-
TACCTCGTATACACTGAGAGAGGTTGAACTGAGAATCATGGATGAAAA
GGCCTGTGTGGACTACAGGTATTATGAATACAAATTCCAGGTCTGCGT
GGGCAGTCCCACAACTTTAAGAGCAGCATTCATGGGAGACTCTGGCG-
GACCGCTACTGTGTGCTGGTGTGGCTCATGGTATTGTATCTTATGGG-
CATCCAGATGCAAAGCCCCCTGCAATCTTCACCCGAGTCTCCACATA
TGTGCCCTGGATTAATGCAGTCATTAATACAAGTAGCGGCCGC.

In situ hybridization was performed on 5 μm sections of formalin-fixed, paraffin embedded LV tissue from rats using the antisense rMcpt2 probe. The sense probe was used as a control. After removal of paraffin with clean xylene, tissue sections were rehydrated through a series of ethanol and diethylpyrocarbonate-treated water washes. All solutions were appropriately treated to remove nucleases. The sections were immersed in 0.2M HCl at room temperature for 20 minutes, rinsed with 0.2% glycine in PBS, and digested in 20 μg/ml proteinase K (Boehringer Mannheim) at 37 °C for 20 minutes. After washing with 0.2% glycine, the sections were immersed in 5% concentrated Trilogy stock (Cell Marque) in Milli-Q water and boiled for 15 minutes at 121 °C in an autoclave (Tuttnauer 2340M, Mohaweek Medical Mall). After washing with 0.2% glycine and 2×SSC (1×SSC consisting of 150 mM NaCl and 15 mM sodium citrate, pH 7.0), each section was prehybridized at 60 °C for 2 hours with prehybridization buffer (50% formaldehyde, 2×SSC, 1×Denhardt's solution, 1 mM EDTA, 100 μg/ml heat-denatured salmon sperm DNA). Hybridization was carried out in hybridization buffer (50% formaldehyde, 2×SSC, 1×Denhardt's solution, 1 mM EDTA, 10% dextran sulfate and 350 μg/ml heat-denatured salmon sperm DNA). The labeled RNA probe (100 nanograms) was diluted in 100 μl of hybridization buffer and denatured for 5 minutes at 95 °C and immediately chilled on ice to prevent reannealing. Hybridization was carried out in a humidity chamber at 60 °C for 16 hours. Post-hybridization washes consisted of 2×SSC, 1×SSC and 0.1×SSC with gentle agitation and washed twice, respectively. All washes were carried out at 45 °C for 30 minutes. Sections were then blocked in blocking buffer (10% heat inactivated goat serum, 1% Boehringer Block and 0.1% Tween-20) for 2 hours at room temperature. Sections were incubated overnight at 4 °C with an anti-Digoxigenin-AP fab fragments antibody (Roche, 11093274910) conjugated with alkaline-phosphatase diluted at 1:2000 in blocking buffer then stained using the BM purple substrate (Roche, 11442074001) for alkaline phosphatase. The slides were then mounted on coverslips and viewed under a Leica DM6000 epifluorescence microscope.

2.7. mRNA quantitation by RT-PCR

Total RNA of isolated rat cardiac cardiomyocytes was extracted from 3, 24 hour, 4 and 12 week sham and ACF rats using RNeasy Mini Kit (Qiagen, #74106) as previously described [6]. Briefly, mRNA transcripts of chymase were evaluated by real time RT-PCR using Assay-On-Demand primer mix of rMcpt2 (rMcpt2, rat mast cell protease 2, assay ID: Rn00756479_g1). Ribosomal protein, large, P0 (Rplp0; assay ID: Rn00821065_g1) was used in parallel as an internal control. TaqMan One-Step RT-PCR reactions were performed in 20 µl final volumes containing 5 µl ($10\times$ dilution of stock) of RNA sample, AmpErase UNG ($2\times$, 10 µl), MultiScribe reverse transcriptase and RNase inhibitor ($40\times$, 1 µl), primers and probe ($20\times$, 1 µl), and RNase-free water (3 µl). Quantitative real-time PCR was performed using the ABI PRISM 7500 sequence detection system. rMcpt2 mRNA levels relative to sham were calculated using the $\Delta\Delta$Ct method.

2.8. Chymase uptake and myosin breakdown in adult rat cardiomyocytes

Adult rat cardiomyocytes were plated on laminin. The medium was replaced with serum-free medium containing either 0.1% DMSO (vehicle control) or 30 µM Dyngo-4a (Selleckchem, MA) and incubated in a 37 °C tissue-culture incubator for 30 minutes. Recombinant human chymase (2.5 µg/ml, Sigma-Aldrich, MO) or transferrin-Alexa 594 (5 µg/ml, Life Technologies, OR) was added to the medium and incubated for an additional 2 hours at 37 °C. The cells were chilled on ice, and washed three times with PBS, then PBS + 0.5M NaCl, and 3 final PBS washes, and then fixed with 4% paraformaldehyde in PBS for 30 minutes. The uptake of recombinant human chymase was identified with the human chymase antibody (1:50, Abcam ab2377) with the appropriate secondary antibody Alexa Fluor-594 (1:700, Invitrogen). A separate cohort were lysed in RIPA buffer containing Halt protease inhibitor cocktail (PIERCE), and separated on a Novex™ 6% Tris-glycine gel (Invitrogen) under reducing conditions. Proteins were transferred to a PVDF membrane and probed with myosin heavy chain antibody (1:100, DSHB MF-20) and HRP conjugated secondary antibody (GE Healthcare) then developed with Supersignal West Dura Substrate (PIERCE). Equal loading was confirmed by colloidal blue staining (Invitrogen).

2.9. Development of the rMCP-2 antibodies

In previous studies, we focused on rMCP-2 (referred to as chymase from hereon) since it is the most closely related to an Ang II generating rat chymase, vascular smooth muscle chymase [17]. In addition, analysis of a rat mast cell line, RBL-2H3, revealed that degranulation of these cells and analysis of the supernatant by mass spectrometry resulted in 2 major products released, rat mast cell protease 2

(rMCP-2; chymase; ~27 kD) and actin (43 kD) (Fig. 1). Rat MCP-2 polyclonal and monoclonal antisera were developed using a rMCP-2 peptide immunogen (CWGKTGVRDPTSYTLR) which was synthesized and conjugated to two proteins, BSA and KLH. The N-terminal C was added for conjugation of the peptide. The peptide synthesis, conjugation to carrier proteins, and antibody development was performed by Bio-synthesis, Inc. (Lewisville Texas). Twenty eight antibodies were developed by the Hybridoma Cores Facility at UAB, and after further analysis, clone 3F4.5 and a rabbit polyclonal was selected. Immunoabsorption of 3F4.5 and the rabbit antibody with the rMCP-2 peptide blocked staining in an immunohisto-chemistry experiment. Western blot confirmed that the 3F4.5 mouse monoclonal antibody and the rabbit polyclonal antibody recognized the intact recombinant rMCP-2 protein (Cusabio Technology, Inc., Houston, TX) and did not cross react with rMCP-1, rMCP-4 or purified human chymase (Fig. 2).

2.10. Extraction of tissue chymase

A modified extraction method [21, 22] was used to isolate tissue chymase. Briefly, frozen tissue from the LV mid-wall (freshly isolated 2—3 mm^3 pieces, snap frozen in liquid nitrogen and stored at −80 °C) was ground up under liquid nitrogen using a mortar and pestle. 10—20 mg of ground tissue was homogenized in 1 mL of ice cold low salt buffer (10 mM Tris-Cl, pH 8.0, 1 mM EDTA containing enzyme inhibitors — see Table 1) then subjected to a freeze (liquid nitrogen for 2 minutes)/thaw (37 °C water bath for 4 minutes) cycle five times to break up cells and tissue compartments. The lysate was centrifuged at 16,000 × g for 30 minutes (4 °C) and the supernatant discarded. The pellet was re-suspended in 1 mL of ice cold low salt buffer and incu-bated on a rotator for 3 hours at 4 °C. The lysate was centrifuged at 10,000 × g for 30 minutes (4 °C) and the supernatant set aside (low salt extract). The pellet was re-
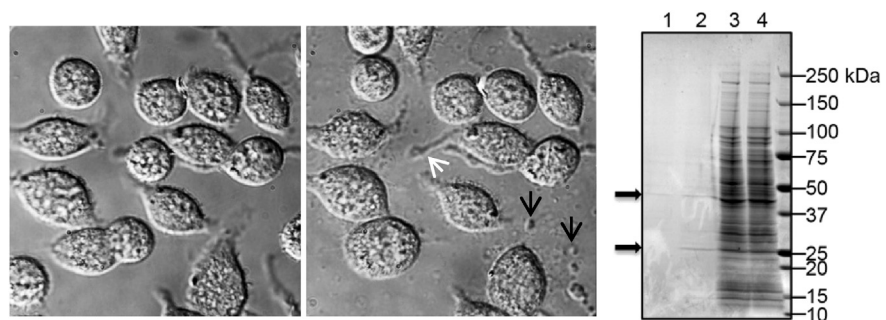

Fig. 1. RBL-2H3 mast cells immediately after addition of ionomycin (5 μg/ml) (middle panel) and 10 minutes after degranulation. Notice membrane projections (white arrow) and released granules and debris (black arrows). MS analysis was performed on whole cell lysates and supernatant after degranulation. Coomassie gel of degranulated (DG) RBL-2H3 demonstrates Lane 1 conditioned media control, Lane 2 conditioned media after DG, Lane 3 is control cell lysate, Lane 4 is cell lysate after DG. Arrows indi-cate a 27 kD band and a 43 kD band which Mass spectroscopy analysis identified as rMCP-2 and actin, respectively. Mass spectroscopy analyses were done through the UAB Mass Spectroscopy Core Facility.
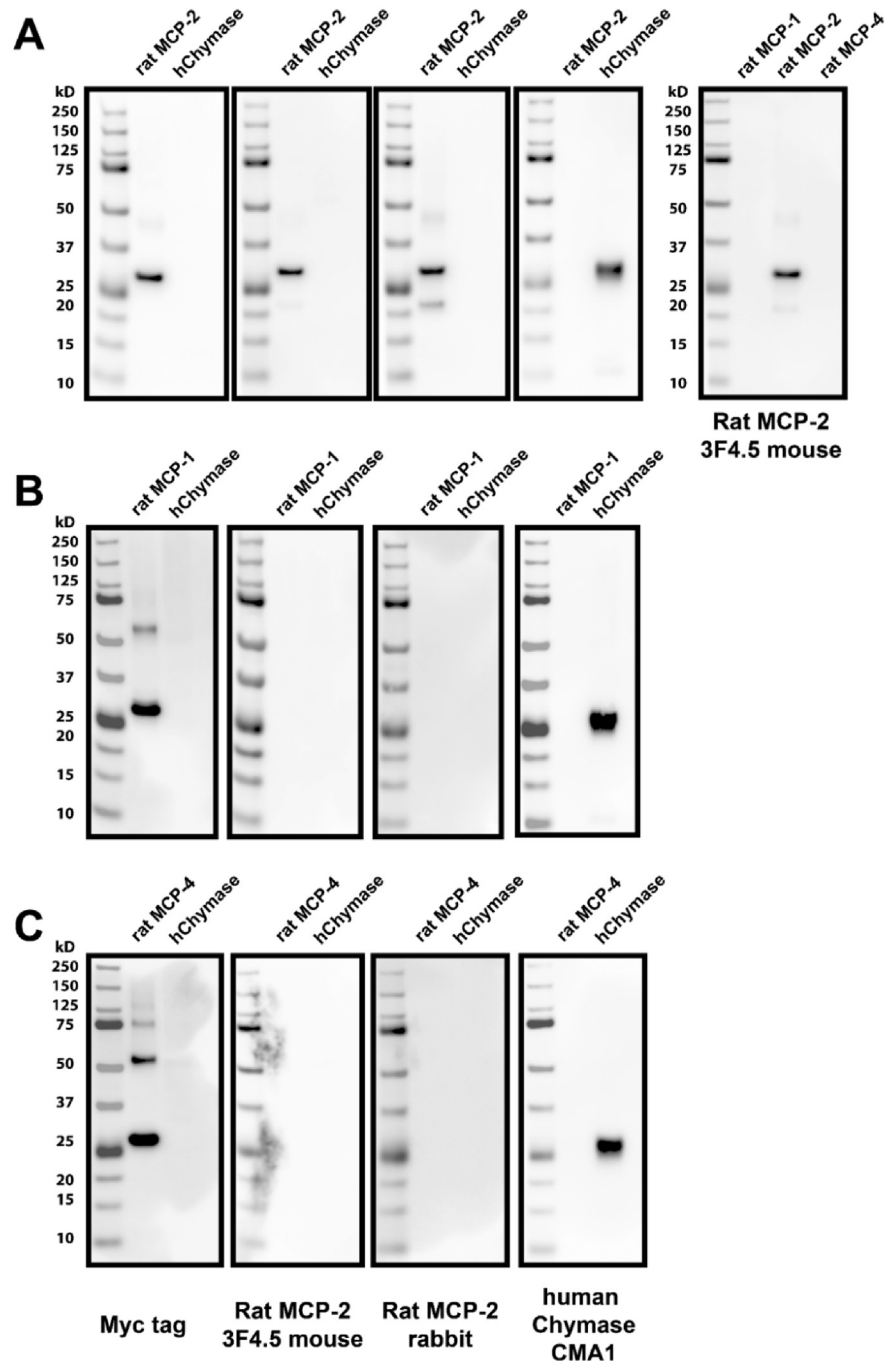
Fig. 2. Western blot showing specificity of custom developed antibodies to Rat MCP-2. The custom 3F4.5 mouse monoclonal and the rabbit polyclonal antibody recognize the intact recombinant rat mast cell protease-2 (rMCP-2) protein (A) and do not cross react with rMCP-1 (B), rMCP-4 (C) or purified human chymase. The recombinant rMCP-1, 2 and 4 have a C or N-terminal Myc tag and the left panel illustrates that the recombinant proteins run at ~27 kD. The 3F4.5 monoclonal and the rabbit polyclonal antibodies recognize the rMCP-2 protein (A − 2nd and 3rd panels) but not purified rMCP-1 (B), rMCP-4 (C) or human chymase (hChymase; 2nd and 3rd panels in each row). The R&D mouse monoclonal recognizes CMA1, the purified human chymase, but not the rMCP-1, 2 or 4 proteins (4th panel). As depicted in the far right panel 3F4.5 specifically recognizes rat MCP-2.

Table 1. Inhibitors used in chymotryptic assay.

Enzyme inhibitor	Final concentration	Supplier	Inhibits
E-64	50 μM	Sigma E3132	Cysteine proteases, trypsin
Pepstatin A	50 μM	Sigma P5318	Acid proteases (aspartyl peptidases)
Bestatin hydrochloride	50 μM	Sigma B8385	Metalloprotease inhibitor (selective leucine aminopeptidase, aminopeptidase B and triamino peptidase)
4-Chloromercuribenzoic acid	50 μM	Sigma C5913	Inhibits enzymes that require unmodified cysteine residues
Lisinopril	50 μM	Sigma L2777	Angiotensin converting enzyme
Amastatin hydrochloride hydrate	10 μM	Sigma A1276	Leucine aminopeptidases
Epoxomicin	1 μM	Sigma E3652	Proteasome

suspended in 1 mL of ice cold high salt buffer (100 mM Tris-Cl, pH 8.0, 1 mM EDTA, 2M NaCl + enzyme inhibitors - see Table 1) and incubated on a rotator for 16 hours at 4 °C. The lysate was then centrifuged at 10,000 $\times$ g for 30 minutes (4 °C) and the supernatant removed (high salt extract) to a separate tube for measurement of chymotryptic activity. Only the high salt extract has chymotryptic activity (data not shown).

2.11. Chymotryptic assay

Chymotryptic enzyme activity was measured in 0.2 mL of high salt extract (containing enzyme inhibitors in Table 1) with the addition of the fluorescent substrate N-Succinyl-Ala-Ala-Pro-Phe-7-amido-4 methylcoumarin at a final concentration of 10 μM (Sigma S9761 − stock solution 7.55 mM or 5 mg/mL dissolved in DMSO). High salt extracts and fluorescent chromophore standards of 7-Amino-4-methylcoumarin (Sigma A9891 − stock of 10 mM dissolved in DMSO; standards were made up in high salt buffer) were run in duplicate on the SpectraMax i3x (Molecular Devices) in a 96-well kinetic plate assay for 1 hour (1 minute interval reads) at 37 °C with an excitation spectrum of 360 nm and emission of 460 nm. To validate chymase specific activity, a separate duplicate containing 50 μM of TEI-F00806 or 50 μM of chymostatin (Sigma C7268) was run in parallel (data not shown). Protein concentration in high salt extracts was quantified with the CB Protein Assay kit (G Biosciences 786-012) with bovine serum albumin (BSA) as the standard. BSA standards were diluted in the same high salt buffer containing enzyme inhibitors. Chymotryptic activity was expressed as fmol/mg/min.

2.12. Western blotting

Recombinant rat mast cell protease 1(rMCP-1; 35 ng Cusabio Technology LLC #CSB-EP357723RA), 2(rMCP-2; 35 ng, Cusabio Technology LLC #CSB-EP360441RA), 4(rMCP-4; 35 ng, Cusabio Technology LLC #CSB-EP311424RA), purified human skin chymase (50 ng, Enzo Life Sciences Inc. #BML-SE281-0000) or rat LV tissue homogenates (2.5 ug) were denatured at 95 °C for 5 minutes in NuPAGE™ LDS Sample Buffer containing NuPAGE™ sample reducing agent (Invitrogen). Samples were separated on a NuPAGE™ Novex 4−12% Bis-Tris (Fig. 2) or 6% Tris-Glycine protein gels (Myosin gels) (Invitrogen), transferred to a 0.2 μm PVDF membrane (Invitrogen) and probed with antibodies to: rMCP-2 antibody (3F4.5 clone; mouse monoclonal; 1:2500; custom see method), rat MCP-2 (rabbit polyclonal; 1:1250; custom see method); anti-Myc tag [9E10] (mouse monoclonal; 1:1000; Abcam #ab32) or anti-human chymase/CMA1 antibody (mouse monoclonal; 1:500; R&D Systems, Inc. #MAB4099), myosin heavy chain MF-20 (mouse monoclonal; 1:400; DHSB) or GAPDH (rat; 1:2500; Abcam #ab9485) for 4 hours at room temperature in 5% BSA (or 5% Blotto for myosin and GAPDH) in phosphate buffered saline + 0.1% Tween-20 (PBST). Membranes were washed in PBST then incubated in horse radish peroxidase (HRP)-conjugated secondary antibodies (Bio-Rad Laboratories; 1:2000−1:5000) for 1−1.5 hours at room temperature in 5% BSA (or 5% Blotto)/PBST. HRP signals were developed using Clarity Western enhanced chemiluminescence substrate (Bio-Rad Laboratories) on a FluorChem M system (Protein Simple).

2.13. Statistical analysis

All data were presented as mean ± SEM (standard error of mean). Spearman correlation analyses were performed to examine linear relationships between LV chymotryptic activity and echocardiographic dimensions using SAS version 9.4 (SAS Institute Inc., Cary, NC, USA). An unpaired Student's t-test was used to compare age-matched shams versus ACF rMcpt2 transcripts and western blot of myosin:-GAPDH. A p value of less than 0.05 was used for statistical significance.

3. Results

3.1. Increased chymase within cardiomyocyte with VO

Previous studies have demonstrated significant LV dilatation in ACF rat hearts at the 4 and 12 week LVs with myofibrillar degeneration and desmin loss [7, 8]. There is a marked increase in rMCP-2 (chymase) within LV cardiomyocytes and interstitial cells (white box) at 24 hours of ACF by immunohistochemistry (IHC) along with a patchy breakdown of desmin versus sham rats [8] that persists at 4 and 12 week ACF (Fig. 3). Sham animals did not exhibit loss of desmin at any time point
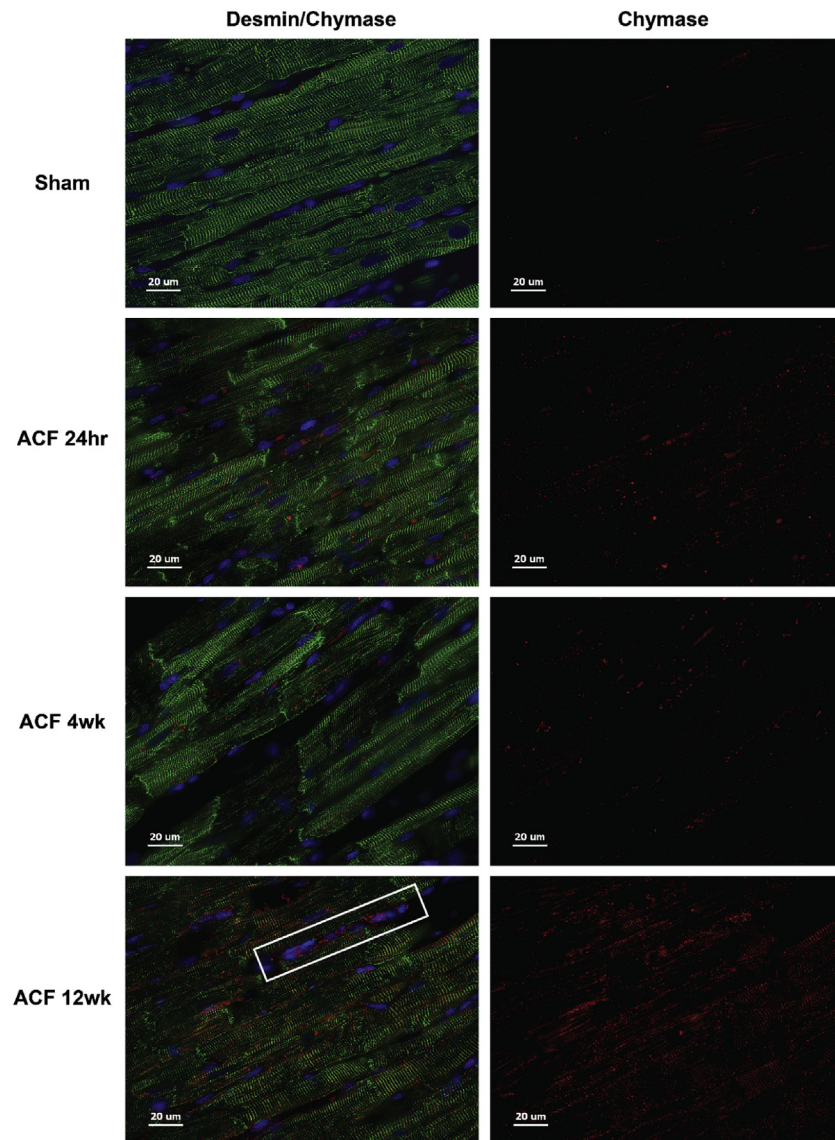
Fig. 3. Immunohistochemistry of Desmin and Chymase in ACF rats. Rat LV sham (4 weeks) and ACF at 24 hours, 4 and 12 weeks (wk) demonstrate desmin (green) breakdown and chymase (red) within cardiomyocytes and interstitial cells. Box indicates chymase labeling in interstitial cells.

(Fig. 4) and a representative sham at 4 weeks is shown in Fig. 3. In addition, LV chymotryptic activity is related to the extent of LV dilatation measured by echocardiographic LV end-diastolic dimension or end-diastolic volume (Fig. 5).

3.2. Transmission electron microscopy (TEM) immunogold labeling of chymase in cardiomyocyte

Fig. 6 demonstrates immunogold TEM in 4-week rat ACF LV cardiomyocytes. Chymase (arrow heads) is located in the z-disc (arrows) and myofibrils of a single
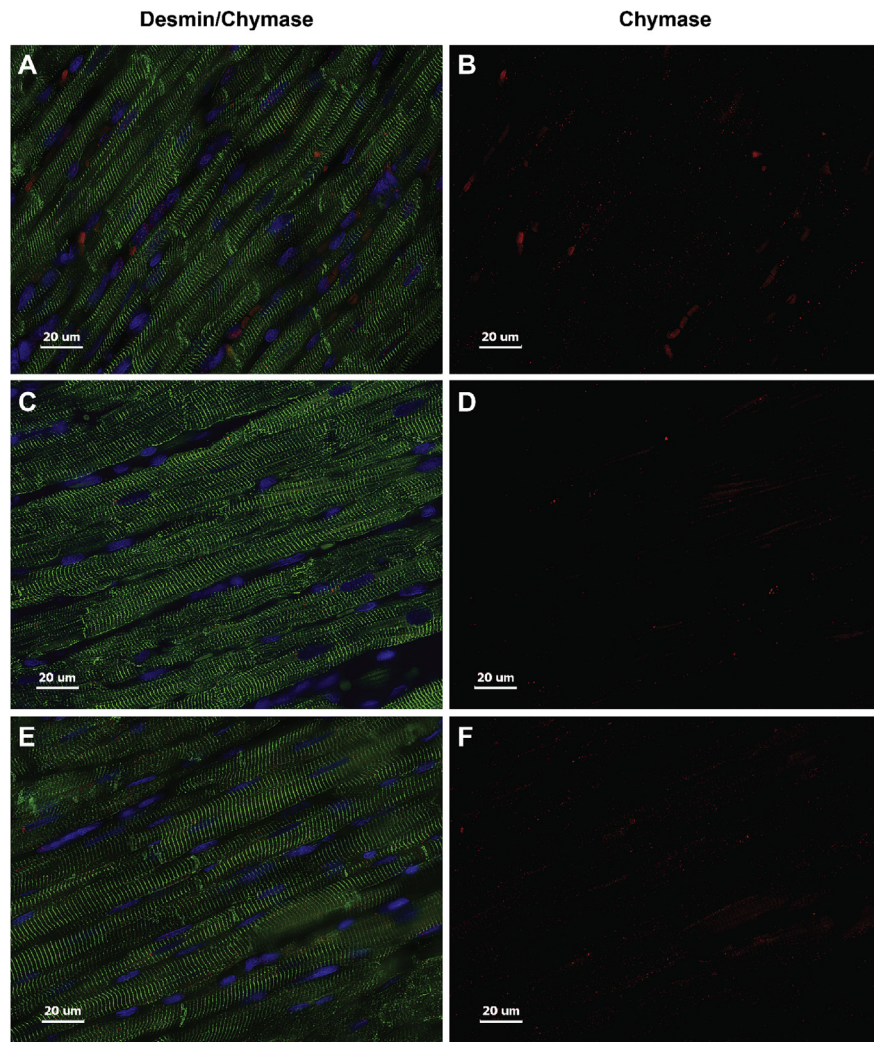
Fig. 4. Immunohistochemistry of Desmin and Chymase in Sham rats. LV Sham animals at 24 hours (A, B), 4 (C, D) and 12 weeks (E, F) demonstrate desmin (green) and chymase (red) within cardiomyocytes showing no difference in staining patterns at all-time points.

sarcomere, mitochondria (mito) and nucleus (box) as indicated by the IHC image LVs in Fig. 3.

3.3. In situ chymase activity in LV tissue with VO

Activity of chymase within cardiomyocytes is verified by *in situ* chymotryptic activity where chymase-like activity is identified by diffuse blue dots in a 4-week sham (Fig. 7A) versus a 4-week ACF rat (Fig. 7B). The blue dots can be seen between the striations of the representing z discs associated myofibrils as seen in the TEMs in Fig. 6. The increased chymotryptic activity is prevented by pretreatment with the specific chymase inhibitor (C). Fig. 7D demonstrates an LV cross-section with an intensely stained degranulating mast cell with staining in the adjacent
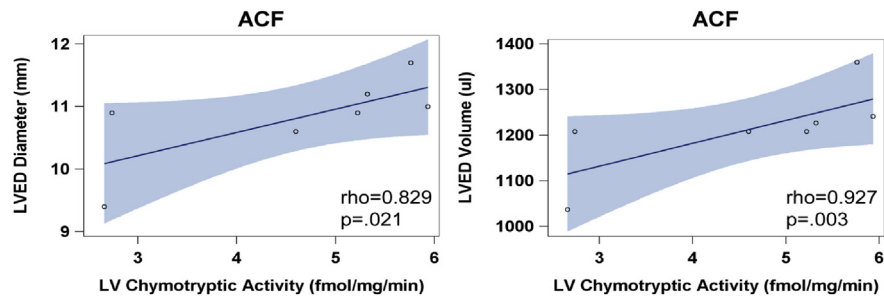
Fig. 5. LV tissue chymotryptic activity correlates with LV dysfunction in ACF rats at 4 and 12 weeks. LV chymotryptic activity (fmol/mg/min) is related to the extent of LV dilatation measured by LV end-diastolic (ED) diameter and LVED volume. Blue shading represents the 95% confidence intervals.

cardiomyocytes indicative of intracellular chymotryptic activity. IHC inset shows the red chymase granules within a mast cell and adjacent cardiomyocyte. The patchy blue dot staining coincides with the chymase staining by IHC in Fig. 3 and chymase by TEM immunogold in Fig. 6 in a 4-week ACF LV. Taken together, these data demonstrate the presence and activity of chymase within cardiomyocytes and mast cells.

3.4. Chymase production by endothelial cells and fibroblasts with VO

In situ hybridization of 4-week ACF LV cross section demonstrates chymase mRNA (anti-sense) located in interstitial cells and in endothelial cells (Fig. 8A) with negative in the control (Fig. 8B, sense probe). IHC of LV cross-section from a 4-week ACF (Fig. 8C) demonstrates rMCP-2 in interstitial cells of ACF LV with mast cells (arrows) and other interstitial cells (arrow head) and endothelial cells lining a blood vessel (arrow head). Isolated cardiomyocytes from a 12 week ACF (Fig. 8D) rat demonstrates both endothelial cells (arrow head) with chymase (red) co-staining with von Willebrand factor (green) specific for endothelial cells. Real-time PCR of isolated cardiomyocytes from 3 hours, 24 hours, 4-week and 12 week ACF LVs shows low levels and no increase in rMCP-2 mRNA (Fig. 8E). However, endothelial cells and fibroblasts may contribute to the chymase mRNA, thereby further supporting *in situ* hybridization results in which there is little to no cardiomyocyte chymase mRNA.

3.5. Myofibrillar breakdown and myosin fragmentation in ACF

Myofibrillar breakdown has been reported in the human with chronic isolated MR [9, 23] and in the dog [18] with experimentally-induced chronic MR by hematoxylin and eosin staining and transmission electron microscopy. Fig. 9 demonstrates a sarcomeric registry of myosin (red) between z-discs defined by desmin (green) in the 4-week Sham rat. There is no difference in Sham animals at 24 hours, 4 or 12 weeks
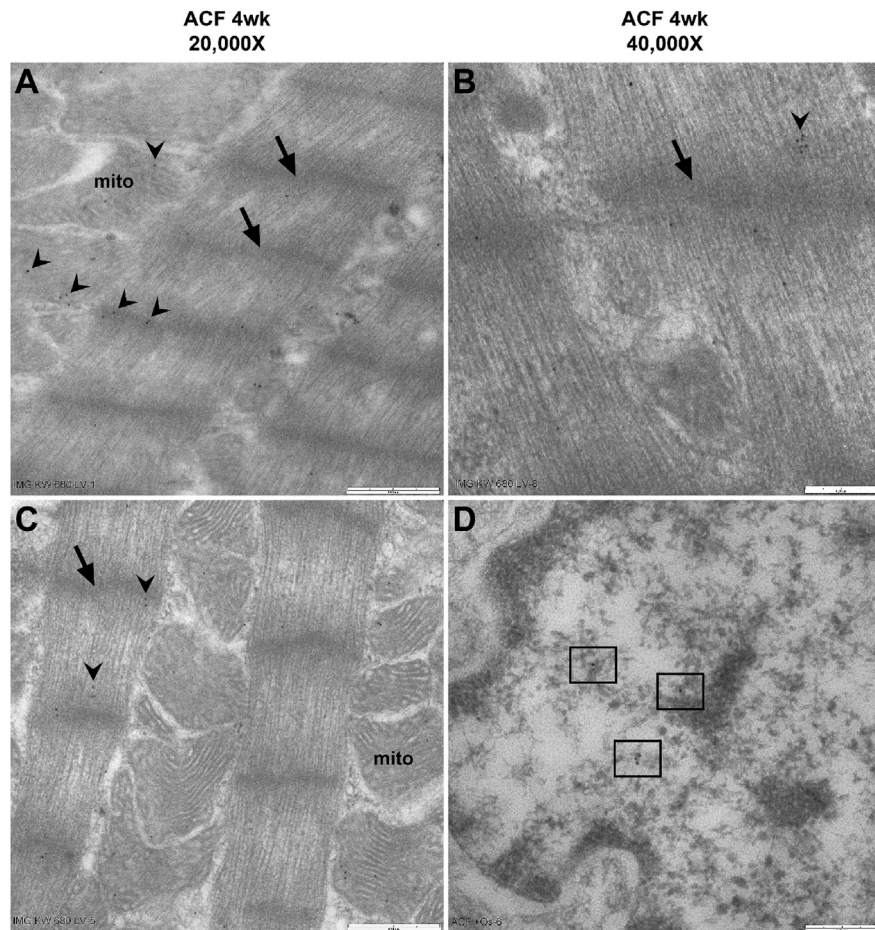
Fig. 6. TEM immunogold labeling of Chymase in ACF rats. In 4 week (wk) ACF rat, immunogold labeling of chymase (black dots, arrowheads) at 20,000X (A and C; bar = 0.5 um) and 40,000X (B and D; bar = 0.25 um) indicating association with myofibrils between z-discs (arrows) and in mitochondria (mito). Panel D demonstrates chymase (black dots within boxes) in a cardiomyocyte nucleus.

(Fig. 10). Coincident with cardiomyocyte chymase infiltration in ACF (Fig. 3), there is a corresponding loss of myosin and desmin staining starting at 24 hours and persisting at 4 and 12 weeks of ACF (Fig. 9). In addition, myosin is significantly decreased in 4-week ACF versus sham animals by western blot (Fig. 11).

3.6. Chymase uptake and myosin degradation in isolated adult rat cardiomyocytes

Fig. 12 shows human chymase uptake by cardiomyocytes (Fig. 12A, middle panel) that is attenuated by pretreatment with Dyngo-4a (30 μM) (Fig. 12A, far right panel). The Dyngo-4a pretreatment blocks transferrin uptake by transferrin receptor (control), a receptor known to require dynamin for uptake (Fig. 12B). The results illustrate that chymase is rapidly taken up by cardiomyocytes through a dynamin-mediated endocytic process. Dyngo-4a pretreatment results in an attenuation of
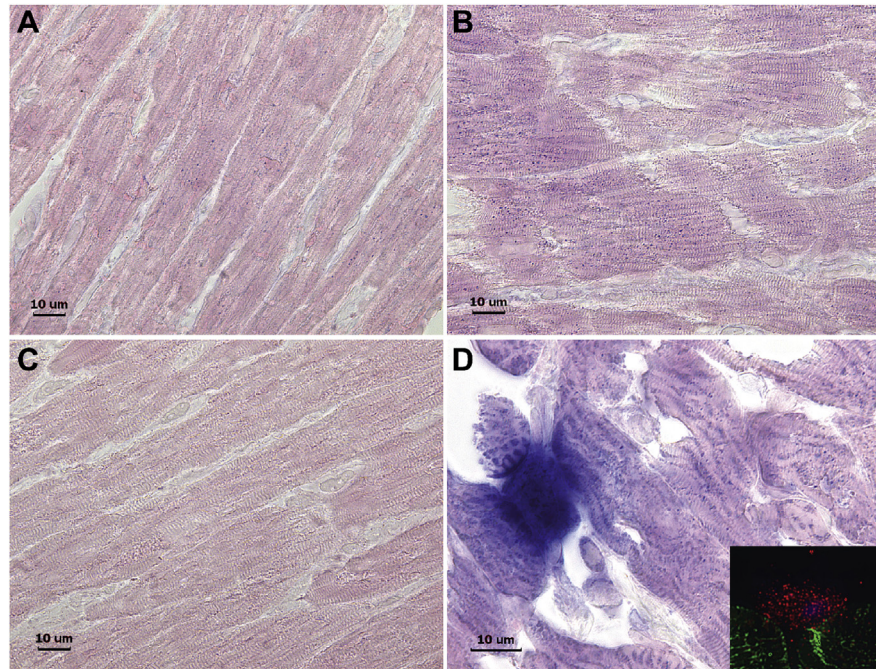
Fig. 7. In-Situ tissue chymotryptic activity. Increased chymotryptic activity in LV cardiomyocytes of ACF (B) versus 4 week sham (A) and intense blue staining in a mast cell and in adjacent cardiomyocytes in cross section [D and by IHC inset, desmin (green), chymase (red)]. Chymotryptic activity is prevented by pretreatment of tissue with a chymase inhibitor - TEI-F00806 (C).

myosin breakdown (Fig. 12C) and is consistent with the hypothesis that chymase up-take is in part required for myosin breakdown.

3.7. Chymase inhibition prevents myosin breakdown in the dog with chronic isolated MR

We have previously reported that chymase inhibition prevents myofibrillar break-down in the dog with four months of isolated MR [18]. As in the rat with ACF (Fig. 3), in Fig. 13 there is an increase in cardiomyocyte chymase and desmin break-down within dog MR cardiomyocytes versus normal (NL) best demonstrated in the chymase alone images (right panels). Fig. 14 demonstrates that breakdown of des-min and myosin in the untreated MR dog heart is attenuated by treatment with an oral chymase inhibitor (CI) for 4 months after induction of MR.

4. Discussion

The current study demonstrates the extensive presence of chymase within cardio-myocytes early and throughout the course of a pure VO and addresses questions regarding its source as well as its potential role in mediating myofibrillar breakdown and adverse remodeling of the cardiomyocyte and LV in a pure VO.
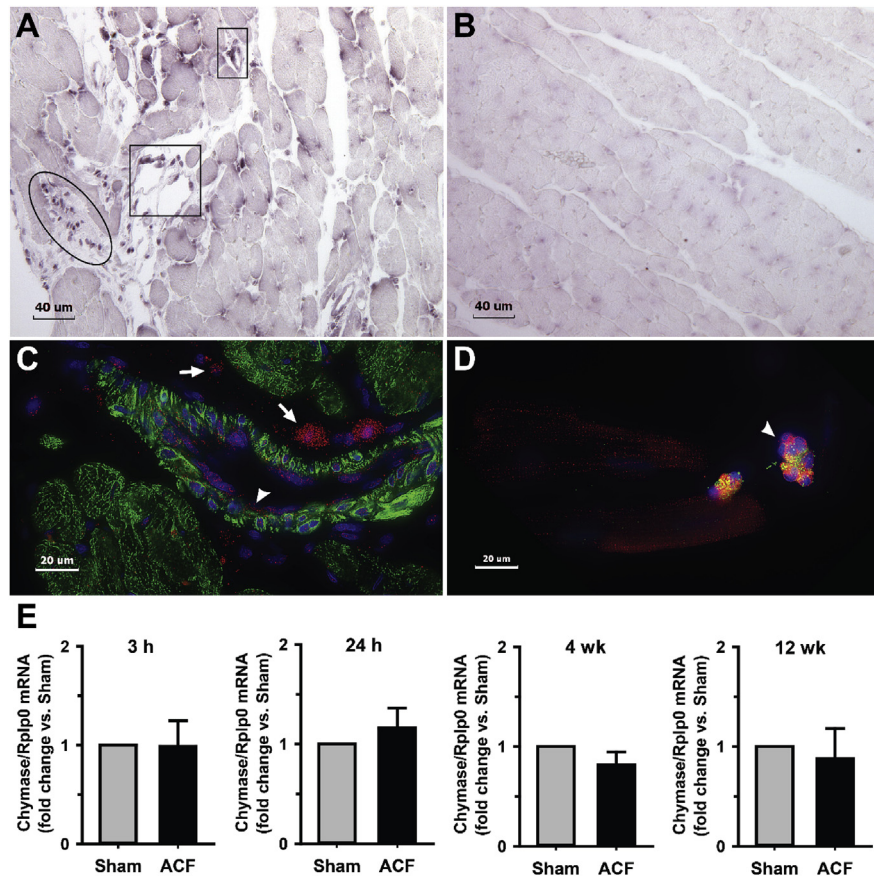
Fig. 8. *In situ* hybridization of Chymase mRNA in ACF rats. Anti-sense (A) and sense (B) chymase mRNA in rat interstitial cells (oval) and endothelial cells of vessels in cross-section (boxes) in the LV of 4 week ACF animals. Cross-section IHC of ACF LV (C) demonstrates chymase (red) in endothelial cells of blood vessel (arrow head) and interstitial cells and mast cells (arrows) with chymase (red) with desmin (green) and DAPI stain of nuclei (blue). IHC of isolated 12 week ACF cardiomyocytes (D) with intracellular chymase (red) and chymase within endothelial cells (arrow head) identified by von Wille-brand factor (green). Chymase mRNA from LV cardiomyocytes of age-matched sham and ACF at 3 and 24 hours (h) and 4 and 12 weeks (E). n = 6 hearts per group.

Chymase has many proteolytic functions that mediate acute tissue injury and chronic remodeling that have been largely attributed to its actions in the extracellular space due to mast cell activation and degranulation [14]. In this study, we demonstrate extensive rMCP-2 within cardiomyocytes during VO that starts as early as 24 hours and persists at later stages of 4 and 12 weeks. TEM immunogold demonstrates rMCP-2 associated with myofibrils and within the z-disc, mitochondria, and nucleus of VO cardiomyocytes.

In situ hybridization demonstrates that endothelial cells and fibroblasts, in addition to mast cells, are a source of rMCP-2 mRNA. Real-time PCR of isolated adult rat cardiomyocytes produce little rMCP-2 mRNA, some of which may have been due to the inability to completely exclude endothelial cells and fibroblasts from the
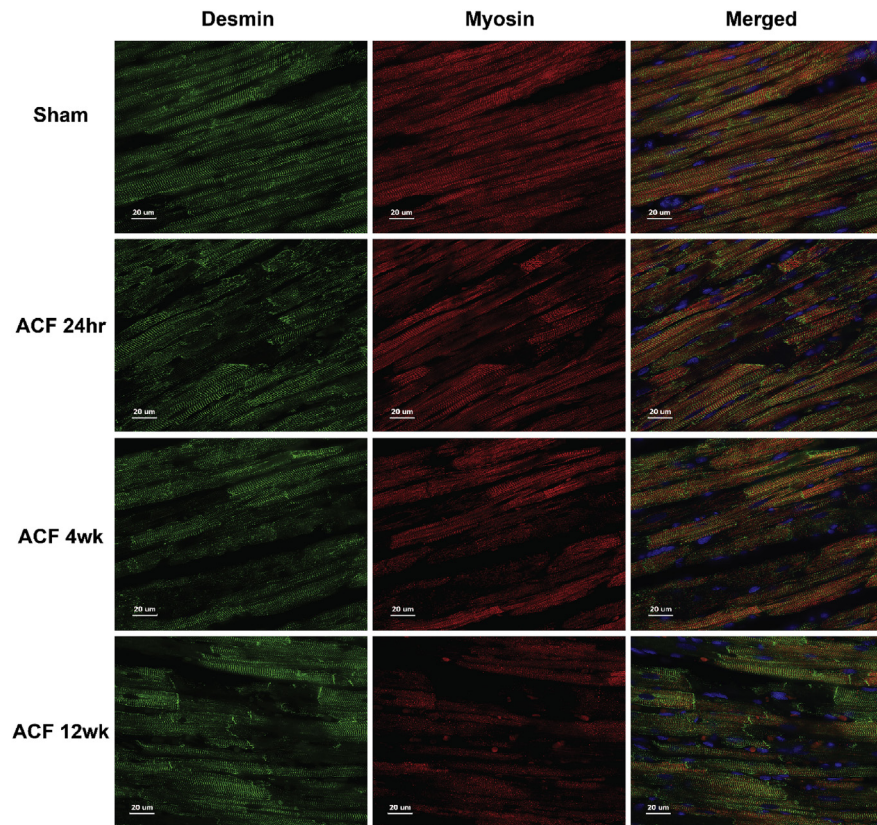
Fig. 9. Immunohistochemistry of Desmin and Myosin in ACF rats. Desmin (green) and myosin (red) and merged LV images in Sham at 4 weeks and ACF LVs at 24 hours (hr), 4 and 12 weeks (wk). Sham hearts have a normal registry of myosin between desmin defined by z-discs that is disrupted in ACF cardiomyocytes.

purification. This is consistent with our previous work in VO of stretched cardiac fibroblasts [6] and chymase mRNA production from endothelial cells and other interstitial cells in the failing human heart [24].

In situ chymotryptic activity allowed for an examination of chymase/chymotryptic-like activity within intact cardiomyocytes without disrupting the compartmentalization of chymase. The *in situ* images demonstrate chymotryptic activity within VO cardiomyocytes that is most intense in cardiomyocytes adjacent to chymase abundant mast cells and blocked by pretreatment with a chymase inhibitor. Figs. 3, 6, and 7 suggest a movement of chymase into cardiomyocytes during ACF with intracellular function manifested by *in situ* chymotryptic activity. Our *in situ* hybridization results further support the contention that the increased cardiomyocyte chymase is largely due to uptake from adjacent fibroblasts, endothelial cells and mast cells rather than *de novo* cardiomyocyte synthesis.

We have examined the effects of adding human chymase to HL-1 cells [15], adult rat and cardiac fibroblasts [6]. In HL-1 cells, we have shown that entry of active
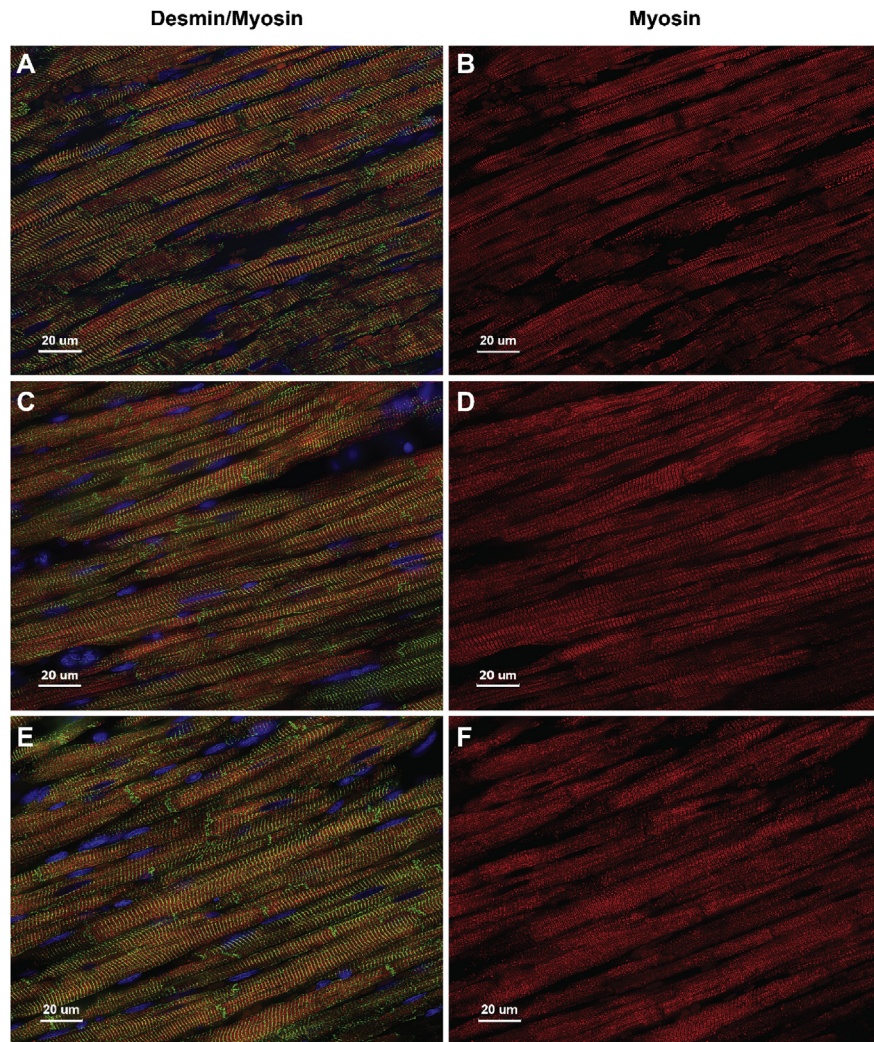
Desmin/Myosin   Myosin

Fig. 10. Immunohistochemistry of Desmin and Myosin in Sham rats. LV Sham rats at 24 hours (A,B), 4 (C,D) and 12 weeks (E,F) demonstrate desmin (green) and myosin (red) within cardiomyocytes showing no difference in staining patterns at all-time points. Fig. 9 in the manuscript shows a representative age-matched sham rat at 4 weeks.

chymase results in NR4 translocation from nucleus to cytoplasm, mitochondrial damage and breakdown of myosin—all of which are attenuated by a dynamin inhibitor that prevents chymase uptake [15]. Many of these functional effects of chymase *in vitro* are prevented by chymase inhibition in I/R [15] or MR [18] dogs *in vivo*. In the adult rat cardiac fibroblast [6], chymase is again internalized through a dynamin-dependent mechanism and leads to an increased formation of autophagic vacuoles, LC3-II production and autophagic flux, resulting in increased procollagen degradation [6]. Cyclical stretch of fibroblasts induces the same autophagic-mediated procollagen degradation that is prevented by pretreatment with chymase inhibitor [6]. Here we demonstrate an increase in chymase
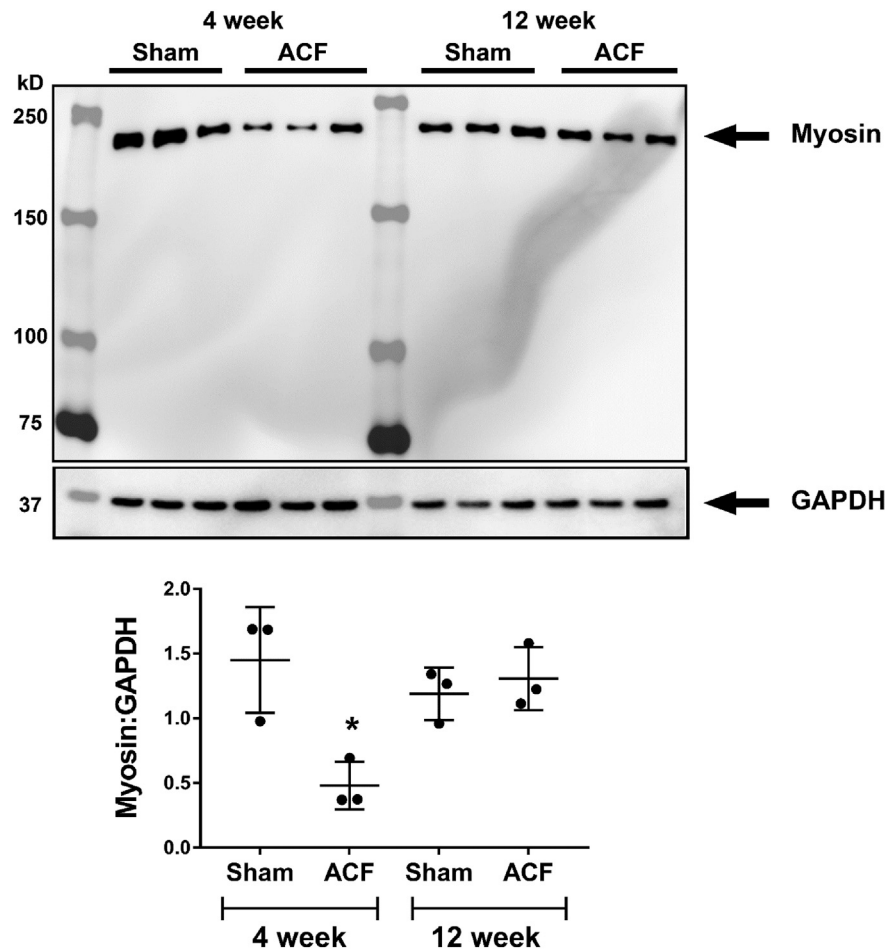
Fig. 11. Western immunoblot of myosin heavy chain in rat LV tissue in Sham and ACF rats at 4 and 12 weeks. Total myosin heavy chain (230kD) is significantly decreased in 4 week ACF rats versus age-matched sham rats (*p < 0.05, Student t-test). However, there is no significant difference between Sham and ACF rats at 12 weeks. N = 3 rats per group.

within the rat cardiomyocytes concomitant with myosin breakdown, both of which are attenuated by pretreatment with a dynamin inhibitor. In another study, a chymase inhibitor (chymostatin) and Ang-(1−12) dialyzed into an adult rat cardiomyocyte prevented the subsequent effect on potassium currents. This treatment is also prevented when an AT_1 receptor blocker is delivered with Ang-(1−12) intracellularly, but not when added extracellularly, supporting an intracellular chymase-mediated Ang II/AT_1 receptor activation process [25]. Taken together, these studies demonstrate physiological effects that are linked to chymase actions in the cardiomyocyte.

There are limitations for testing currently available chymase inhibitors in a clinically relevant fashion in rodent models *in vivo*. The human has only one α-chymase isoform which has served as the platform for design of multiple available chymase
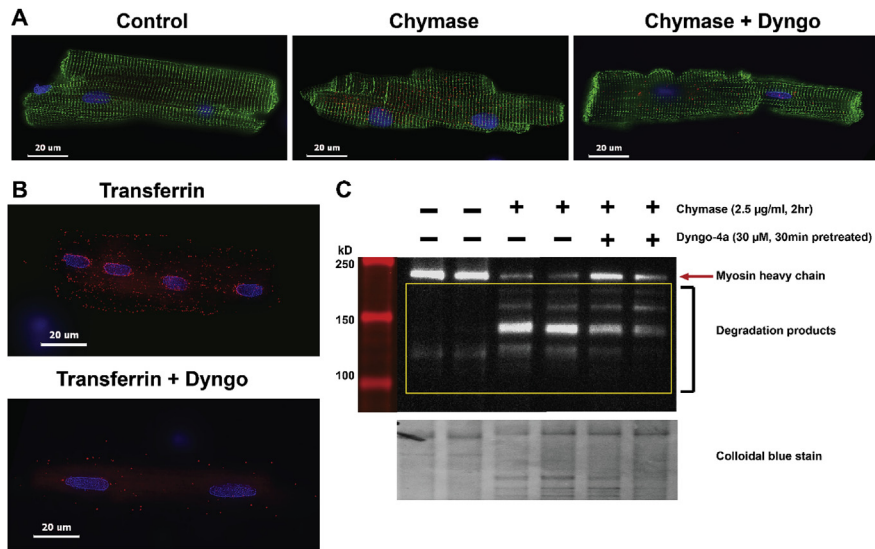
Fig. 12. Chymase uptake in isolated rat cardiomyoctes. Human chymase added to adult rat cardiomyoctyes (desmin, green) shows chymase (red) uptake (A) is attenuated by pretreatment with Dyngo-4a (30 μM), an inhibitor for dynamin. Dyngo-4a pretreatment blocks transferrin (red) uptake (B). Dyngo pretreatment attenuates myosin breakdown as shown by western blot (C) with a corresponding decrease in chymase uptake.
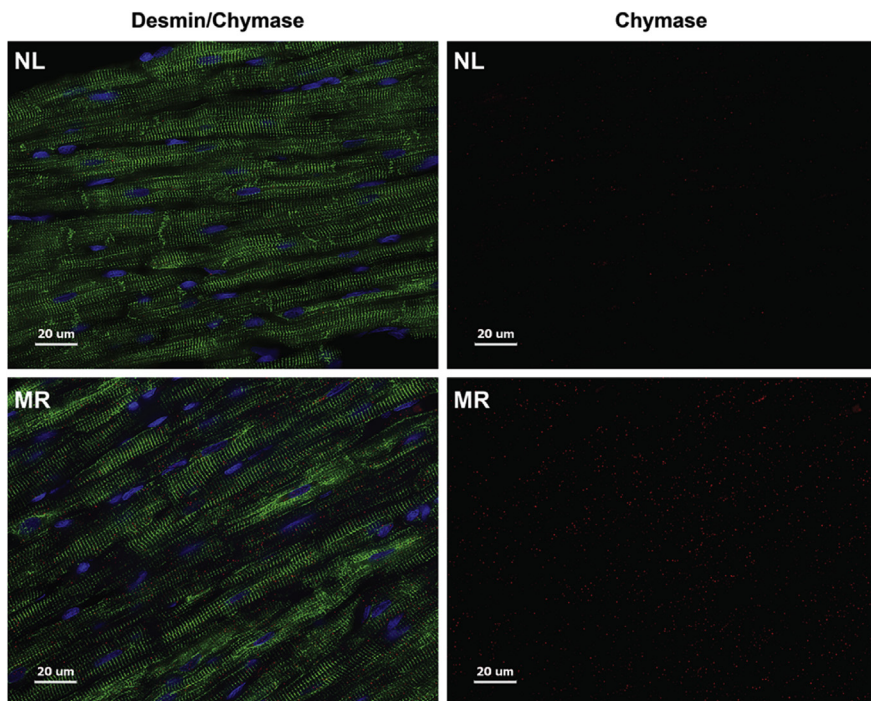

Fig. 13. Immunohistochemistry of Desmin and Chymase in the MR dog. Desmin (green) and chymase (red) merged (left panels) and chymase alone (right panels) in normal (NL) dog versus 4 month MR dog show increased intracellular chymase and desmin loss in the MR dog.
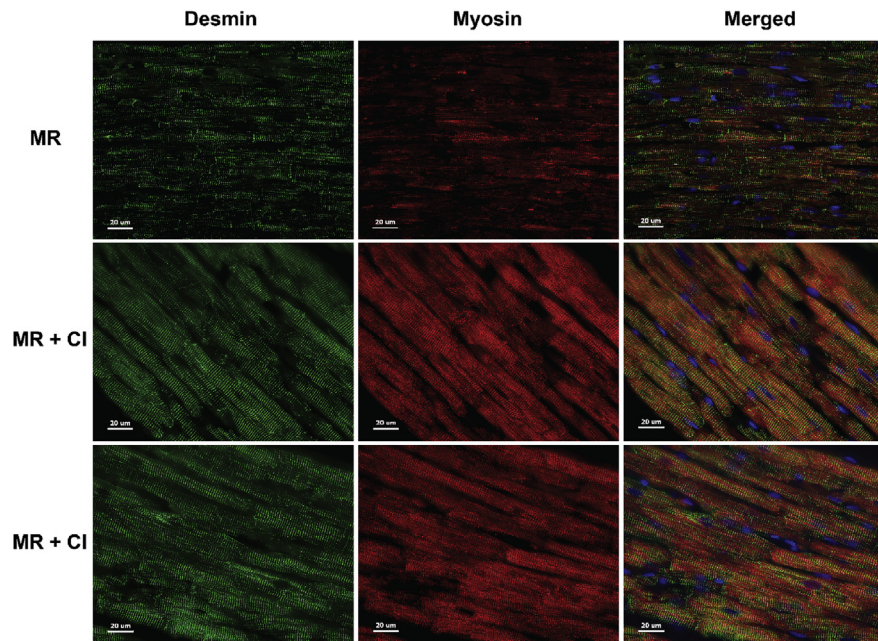
Fig. 14. Immunohistochemistry of Desmin and Myosin in the MR dog. Breakdown of desmin (green) and myosin (red) and merged (far right panels) demonstrated in 4 month MR dogs is blocked by a chymase inhibitor (CI).

inhibitors [26]. Mouse and rat mast cells have α-chymase and multiple β-chymase isoforms that both form and degrade Ang II [17, 27]. A total of 10 rat mast cell proteases have been cloned and four of the ten (rMCP-1, rMCP-2, rMCP-3, rMCP-4) display chymotryptic activities that differ in exact substrate specificity [28, 29, 30, 31]. The functional heterogeneity among rodent β-chymases suggests that they are not redundant proteases but serve distinct roles in mast cell biology and immunity. Although rMCP-1 and rMCP-2 have chymotryptic activity, both cleave at phenylalanine and tyrosine residues efficiently [32, 33] and therefore could potentially degrade Ang II to Ang-(1−4) when Ang II is formed. Furthermore, rMCP-2 has distinct chymotryptic substrate specificities to cell adhesion and cell junction molecules that regulate intestinal permeability via cleavage of occludin, protocadherin alpha 4 and cadherin 17 [33]. Thus, in the rat there are many other targets of the multiple rMCPs that can influence tissue remodeling apart from Ang II formation.

To circumvent the obstacle of β-chymases with their numerous and varied substrate specificity characteristics and achieve greater clinical relevance, we have studied MR in the dog which has a single α-chymase similar to the human and lacks a β-chymase. After 4 months of MR, chymase inhibition results in a significant decrease in LV MMP activation and fibronectin degradation, restoration of the focal adhesion complex, and reduction of myofibrillar loss, resulting in improved LV systolic function and isolated cardiomyocyte shortening [18]. At the time, we attributed these

effects to an inhibition of interstitial chymase activity that starts with degradation of fibronectin and disruption of the focal adhesion complex leading to increased sarcomere disorganization and myofibrillar degeneration [18]. Indeed, chymase added to adult dog cardiomyocytes disrupts the focal adhesion complex [15] and a mouse conditional knockout of FAK results in a similar LV dilatation with cardiomyocyte elongation, wall thinning and myofibrillar breakdown [34]. However, reevaluation of our MR dog hearts now demonstrates a similar large presence of chymase within LV cardiomyocytes with desmin and myosin breakdown that is prevented by chronic chymase inhibition. Taken together, our current *in vivo* and *in vitro* results in the rat and dog support a potential combined outside and inside chymase-mediated mechanism in the cytoskeletal and myofibrillar breakdown with VO.

This study although descriptive in nature along with the inherent problem of multiple β-chymase isoforms in the rodent nevertheless raises interesting questions regarding the intracellular function of chymase that, in addition to Ang II-forming capabilities, also includes multiple destructive protease actions both outside and within the cardiomyocyte [14]. The identification of cellular sources other than mast cells, including cardiac fibroblasts and vascular endothelial cells, demonstrates a more widely dispersed production and distribution system to the cardiomyocyte that also accounts for its relatively high protein abundance in human heart tissue (about 1.3 μg/g) [35]. The clinical relevance is further reinforced by chymase upregulation in the human myocardial infarction heart, vulnerable atherosclerotic plaque, aortic aneurysm, atherosclerosis, and diabetic kidney [14]. Further studies in the human are required to document the intracellular location and function of chymase and its other targets in mediating tissue injury and remodeling. Understanding these chymase functions may address the "residual risk" in clinical trials of cardiovascular disease using conventional renin-angiotensin system blockade [36].

Declarations

Author contribution statement

Pamela C. Powell, Wayne E. Bradley: Performed the experiments; Analyzed and interpreted the data.

Chih-Chang Wei, Lianwu Fu: Performed the experiments.

Betty Pat: Performed the experiments; Wrote the paper.

James F. Collawn, Louis J. Dell'Italia: Conceived and designed the experiments; Analyzed and interpreted the data; Wrote the paper.

Funding statement

Competing interest statement

The authors declare no conflict of interest.

Additional information

No additional information is available for this paper.

References

[1] L.J. Dell'italia, et al., Volume-overload cardiac hypertrophy is unaffected by ACE inhibitor treatment in dogs, Am. J. Physiol. 273 (1997) H961−970.

[2] G.J. Perry, et al., Angiotensin II receptor blockade does not improve left ventricular function and remodeling in subacute mitral regurgitation in the dog, J. Am. Coll. Cardiol. 39 (2002) 1374−1379.

[3] T.D. Ryan, et al., Left ventricular eccentric remodeling and matrix loss are mediated by bradykinin and precede cardiomyocyte elongation in rats with volume overload, J. Am. Coll. Cardiol. 49 (2007) 811−821.

[4] C.C. Wei, et al., Cardiac interstitial bradykinin and mast cells modulate pattern of LV remodeling in volume overload in rats, Am. J. Physiol. Heart Circ. Physiol. 285 (2003) H784−792.

[5] C.C. Wei, et al., Cardiac kallikrein-kinin system is upregulated in chronic volume overload and mediates an inflammatory induced collagen loss, PLoS One 7 (2012) e40110.

[6] L. Fu, et al., Increased fibroblast chymase production mediates procollagen autophagic digestion in volume overload, J. Mol. Cell. Cardiol. 92 (2016) 1−9.

[7] D.M. Yancey, et al., Cardiomyocyte mitochondrial oxidative stress and cytoskeletal breakdown in the heart with a primary volume overload, Am. J. Physiol. Heart Circ. Physiol. 308 (2015) H651−663.

[8] J.L. Guichard, et al., Desmin loss and mitochondrial damage precede left ventricular systolic failure in volume overload heart failure, Am. J. Physiol. Heart Circ. Physiol. 313 (2017) H32−H45.

[9]   M.I. Ahmed, et al., Disruption of desmin-mitochondrial architecture in patients with regurgitant mitral valves and preserved ventricular function, J. Thorac. Cardiovasc. Surg. 152 (2016) 1059−1070 e1052.

[10] L.J. Dell'Italia, et al., Increased ACE and chymase-like activity in cardiac tissue of dogs with chronic mitral regurgitation, Am. J. Physiol. 269 (1995) H2065−2073.

[11] J.A. Stewart Jr., et al., Cardiac mast cell- and chymase-mediated matrix metalloproteinase activity and left ventricular remodeling in mitral regurgitation in the dog, J. Mol. Cell. Cardiol. 35 (2003) 311−319.

[12] G.J. Perry, et al., Genetic variation in angiotensin-converting enzyme does not prevent development of cardiac hypertrophy or upregulation of angiotensin II in response to aortocaval fistula, Circulation 103 (2001) 1012−1016.

[13] S. Ahmad, et al., Chymase-dependent generation of angiotensin II from angiotensin-(1-12) in human atrial tissue, PLoS One 6 (2011) e28501.

[14] L.J. Dell'Italia, J.F. Collawn, C.M. Ferrario, Multifunctional role of chymase in acute and chronic tissue injury and remodeling, Circ. Res. 122 (2018) 319−336.

[15] J. Zheng, et al., Chymase mediates injury and mitochondrial damage in cardiomyocytes during acute ischemia/reperfusion in the dog, PLoS One 9 (2014) e94732.

[16] U.M. Chandrasekharan, S. Sanker, M.J. Glynias, S.S. Karnik, A. Husain, Angiotensin II-forming activity in a reconstructed ancestral chymase, Science 271 (1996) 502−505.

[17] C. Guo, et al., A novel vascular smooth muscle chymase is upregulated in hypertensive rats, J. Clin. Investig. 107 (2001) 703−715.

[18] B. Pat, et al., Chymase inhibition prevents fibronectin and myofibrillar loss and improves cardiomyocyte function and LV torsion angle in dogs with isolated mitral regurgitation, Circulation 122 (2010) 1488−1495.

[19] J.F. Huntley, G.F. Newlands, S. Gibson, A. Ferguson, H.R. Miller, Histochemical demonstration of chymotrypsin like serine esterases in mucosal mast cells in four species including man, J. Clin. Pathol. 38 (1985) 375−384.

[20] G.H. Caughey, et al., Chymase and tryptase in dog mastocytoma cells: asynchronous expression as revealed by enzyme cytochemical staining, J. Histochem. Cytochem. 36 (1988) 1053−1060.

[21] I.T. Harvima, N.M. Schechter, R.J. Harvima, J.E. Fraki, Human skin tryptase: purification, partial characterization and comparison with human lung tryptase, Biochim. Biophys. Acta 957 (1988) 71−80.

[22] I.T. Harvima, et al., Biochemical and histochemical evaluation of tryptase in various human tissues, Arch. Dermatol. Res. 281 (1989) 231−237.

[23] M.I. Ahmed, et al., Increased oxidative stress and cardiomyocyte myofibrillar degeneration in patients with chronic isolated mitral regurgitation and ejection fraction >60%, J. Am. Coll. Cardiol. 55 (2010) 671−679.

[24] H. Urata, et al., Cellular localization and regional distribution of an angiotensin II-forming chymase in the heart, J. Clin. Investig. 91 (1993) 1269−1281.

[25] W.C. De Mello, L.J. Dell'Itallia, J. Varagic, C.M. Ferrario, Intracellular angiotensin-(1-12) changes the electrical properties of intact cardiac muscle, Mol. Cell. Biochem. 422 (2016) 31−40.

[26] J. Kervinen, et al., Potency variation of small-molecule chymase inhibitors across species, Biochem. Pharmacol. 80 (2010) 1033−1041.

[27] G.H. Caughey, W.W. Raymond, P.J. Wolters, Angiotensin II generation by mast cell alpha- and beta-chymases, Biochim. Biophys. Acta 1480 (2000) 245−257.

[28] C. Lutzelschwab, G. Pejler, M. Aveskogh, L. Hellman, Secretory granule proteases in rat mast cells. Cloning of 10 different serine proteases and a carboxypeptidase A from various rat mast cell populations, J. Exp. Med. 185 (1997) 13−29.

[29] U. Karlson, G. Pejler, G. Froman, L. Hellman, Rat mast cell protease 4 is a beta-chymase with unusually stringent substrate recognition profile, J. Biol. Chem. 277 (2002) 18579−18585.

[30] U. Karlson, G. Pejler, B. Tomasini-Johansson, L. Hellman, Extended substrate specificity of rat mast cell protease 5, a rodent alpha-chymase with elastase-like primary specificity, J. Biol. Chem. 278 (2003) 39625−39631.

[31] M.K. Andersson, U. Karlson, L. Hellman, The extended cleavage specificity of the rodent beta-chymases rMCP-1 and mMCP-4 reveal major functional similarities to the human mast cell chymase, Mol. Immunol. 45 (2008) 766−775.

[32] S. Sanker, et al., Distinct multisite synergistic interactions determine substrate specificities of human chymase and rat chymase-1 for angiotensin II formation and degradation, J. Biol. Chem. 272 (1997) 2963−2968.

[33] Z. Fu, M. Thorpe, L. Hellman, rMCP-2, the major rat mucosal mast cell protease, an analysis of its extended cleavage specificity and its potential role in regulating intestinal permeability by the cleavage of cell adhesion and junction proteins, PLoS One 10 (2015) e0131720.

[34] X. Peng, et al., Cardiac developmental defects and eccentric right ventricular hypertrophy in cardiomyocyte focal adhesion kinase (FAK) conditional knockout mice, Proc. Natl. Acad. Sci. U. S. A. 105 (2008) 6638−6643.

[35] H. Urata, A. Kinoshita, K.S. Misono, F.M. Bumpus, A. Husain, Identification of a highly specific chymase as the major angiotensin II-forming enzyme in the human heart, J. Biol. Chem. 265 (1990) 22348−22357.

[36] S. Reyes, et al., Novel cardiac intracrine mechanisms based on Ang-(1-12)/ chymase Axis require a revision of therapeutic approaches in human heart disease, Curr. Hypertens. Rep. 19 (2017) 16.